Hydrodynamics of an airlift reactor for aeration in molten sulfur

Junjie Wang, Xiao Xu*, Qiang Yang*, Wei Wang, Yudong Li, Shihan Wu, Haiqiang Yang

School of Mechanical and Power Engineering, East China University of Science and Technology, *Shanghai 200237*, *China*

(Note: authors marked with * are corresponding authors)

Abstract: An industrial-scale internal loop airlift reactor is used to remove volatile gas from high-viscosity molten sulfur. The effects of the superficial gas velocity and reactor height on the hydrodynamic characteristics were studied. The gas holdup, average bubble diameter, and liquid circulation velocity in the reactor under different conditions were analyzed using computational fluid dynamics simulation. The superficial gas velocity was varied from 0.0056 m/s to 0.05 m/s at a constant reactor height of 15 m. The total reactor height was varied from 5 m to 25 m at a superficial gas velocity of 0.0389 m/s. As the superficial gas velocity increased, the gas holdup increased and the bubble diameter did not change significantly. When the superficial gas velocity exceeded 0.333 m/s, the growth rate of the liquid circulation velocity decreased. As the reactor height increased, the gas holdup did not change significantly, the liquid circulation velocity increased, and the bubble diameter increased. However, the bubble diameter decreased at a reactor height of 25 m. Based on the correlation between the gas holdup and liquid circulation velocity proposed by

Chisti (1988), an optimized correlation between the gas holdup and liquid circulation velocity was developed by considering the influence of the bubble diameter. The results obtained using the proposed correlation were compared with those obtained using the Chisti correlation and simulation.

Keywords: Internal loop airlift reactor; molten sulfur; CFD simulation; gas holdup; bubble diameter; liquid circulation velocity

Introduction

The Claus process is the most widely used technology for the treatment of hydrogen sulfide, which is found in raw natural gas and byproduct gases derived from oil refineries. This process is responsible for approximately 90–95% of elemental sulfur production [1]. However, one of the main challenges in elemental sulfur production is the dissolution of hydrogen sulfide into molten sulfur, followed by its gradual escape into the surrounding environment [2]. Currently, aeration or agitation is the most commonly used method of removing hydrogen sulfide from molten sulfur in China. Air stripping and injected oxygen components contribute to the separation of dissolved hydrogen sulfide from molten sulfur. A suitable flow field of molten sulfur facilitates gas–liquid mass transfer. However, agitation involves rotating equipment with a complex structure, which is not suitable for long-term operation. Thus, a passive mixture reactor has been proposed.

An aeration airlift reactor exhibits liquid circulation and a gas upflow pattern, which provides good mass transfer performance and mixing performance. The airlift reactor

consists of an upward zone and a downcomer. Pressurized air in the form of dispersed bubbles enters the upward zone through the gas distribution device located at the lower part of the airlift zone. The mixing density in the upward zone decreases because of gas entrainment. Thus, the liquid in the downcomer exhibits a continuous downward trend. The liquid flows upward in the upward zone and downward in the downcomer to form a liquid circulation pattern in the entire reactor.

The aeration airlift reactor is a suitable for the removal of dissolved hydrogen sulfide from molten sulfur. The hydrodynamics of the airlift reactor affect the degassing for molten sulfur treatment. However, there are few studies on the hydrodynamics of aeration airlift reactors with the industrial-scale physical properties of molten sulfur. In this study, the air bubble diameter, gas holdup, and liquid circulation velocity were studied through computational fluid dynamics (CFD) and mathematical modeling. The schematic of the airlift reactor is shown in Fig. 1.

The outer column of the airlift reactor had an inner diameter of 1600 mm, and different heights of the column were considered. The inner diameter of the concentric draft tube was 1150 mm. Elliptical heads with a short axis length of 400 mm were placed at both ends of the outer column. Nine gas injection pipes were inserted into the riser. The detailed parameters of the airlift reactor are shown in Table 1.

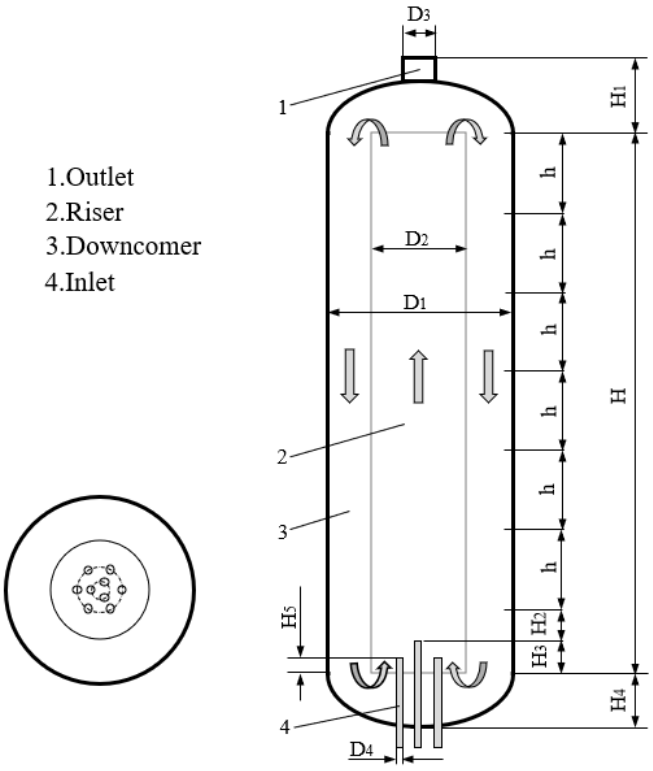

Fig. 1 Schematic of internal loop airlift reactor

Table 1 Parameters of airlift reactor

D1	D2	D3	D4	H1	H2	H3	H4	H5
mm	mm	mm	mm	mm	mm	mm	mm	mm
1600	1150	200	50	600	200	150	400	100

Mathematical modeling

Mathematical modeling provides correlations for hydrodynamic parameters. Chisti and Moo-Yong developed a predictive model for the liquid circulation velocity using the energy balance principle. In their model, energy is input through the isothermal expansion of rising gas bubbles and the kinetic energy of gas sparging [3]. Energy is dissipated via wall friction, the friction and drag forces when the fluid reverses at the

top and bottom zones, bubble wake dissipation, and energy consumption for resisting the buoyancy of bubbles. The model provides a simplified correlation to simultaneously predict the superficial liquid velocity and void fraction in a riser using an iterative procedure [4]. The results obtained using this correlation show better agreement with measurements, as compared with the results obtained using the correlations proposed by Bello et al. and Choi et al. [5].

$$\varepsilon_r = \frac{U_{Gr}}{0.24 + 1.35(U_{Gr} + U_{Lr})^{0.93}} \tag{1}$$

$$U_{Lr} = \left[\frac{2gh_D(\varepsilon_r - \varepsilon_d)}{K_B \left(\frac{A_r}{A_d} \right)^2 \frac{1}{(1-\varepsilon_d)^2}} \right]^{0.5} \tag{2}$$

$$K_B = 11.402 \left(\frac{A_d}{A_b} \right)^{0.789} \tag{3}$$

$$\varepsilon_d = 0.89\varepsilon_r \tag{4}$$

Only the physically relevant root of the polynomial was used. A steady-state value of U_{Lr} was obtained. For the reactor discussed in this work, the value of K_B was 11.7.

The Chisti correlation proposed a correlation that considered the circulation of bubbles in downcomer and does not consider the bubble diameter. The proposed correlation was based on the following assumptions: (1) The bubble diameter varied with the gas flow rate. (2) There was a gas volume fraction in the downflow region.

(3) There were no radial gradients of velocity and density in the liquid and gas phases. (4) The density of the gas phase was constant. (5) The bubble diameter was independent of the reactor height. Generally, liquid viscosity and surface tension decrease as temperature increases. This leads to smaller maximum stable and average bubble diameters and a narrower bubble diameter distribution [6]. (6) The gas holdup was independent of the local height. (7) The conditions in the reactor were isothermal. It should be noted that the temperature of the reactor was maintained as constant because of the cooling by the heat exchanger and the heating of water vapor.

An improved correlation considering the bubble size is necessary which is the aim of our work. The two well-known correlations for the bubble diameter proposed by Akita et al. and Wilkinson et al. are given by equations (5) and (6), respectively. The correlation proposed by Wilkinson et al. is applicable for a large-diameter pipe with large sparger openings, and it accurately predicts the Sauter mean diameter because it considers gas density [7]. Therefore, this correlation is adopted to assess the bubble diameter [8].

$$d_B = 26 D_r \left(\frac{g D_r^2 \rho_L}{\sigma} \right)^{-0.5} \left(\frac{g D_r^3 \rho_L^2}{\mu_L^2} \right)^{-0.12} \left(\frac{U_{Gr}}{\sqrt{g D_r}} \right)^{-0.12} \tag{5}$$

$$\frac{g \rho_L d_B^2}{\sigma} = 8.8 \left(\frac{\mu_L U_{Gr}}{\sigma} \right)^{-0.04} \left(\frac{\rho_L \sigma^3}{g \mu_L^4} \right)^{-0.12} \left(\frac{\rho_L}{\rho_G} \right)^{0.22} \tag{6}$$

According to the two-phase drift flux model derived by Zuber and Findlay [9], the gas velocity in the downcomer can be expressed as follows:

$$U_{Gd} = C_d \varepsilon_d (U_{Gd} + U_{Ld}) - \varepsilon_d U_b \tag{7}$$

where C_d is the distribution parameter that accounts for radial nonuniformity. According to [10], the value of C_d is 1.065.

According to Gao et al., the gas holdup in an airlift reactor is expressed as follows [11]:

$$\varepsilon_r = \frac{U_{Gr}}{1.5(U_{Gr} + U_{Lr}) + U_{Gr} + U_b} \tag{8}$$

It should be noted that the calculated U_{Gr} is composed of two parts [12]: one for gas injection, i.e., $U_{Gr1} = Q_{G,in} / A_r$, and the other for the downcomer, $U_{Gr2} = U_{Gr} - U_{Gr1}$. Thus, the gas velocity in the downcomer can be determined using the continuity equation:

$$U_{Gd} = U_{Gr2} A_r / A_d \tag{9}$$

Jamialahmadi proposed new correlations to predict the terminal velocity of bubbles over a wide range of gas and liquid properties [13]. These correlations are suitable for high temperatures [14].

$$U_b = \frac{U_b^{stokes} U_b^{Mendelson}}{\sqrt{(U_b^{stokes})^2 + (U_b^{Mendelson})^2}} \tag{10}$$

$$U_b^{stokes} = \frac{1}{18}\frac{\rho_L - \rho_G}{\mu_L} g d_{eq}^2 \tag{11}$$

$$U_b^{Mendelson} = \sqrt{\frac{2\sigma}{d_{eq}(\rho_L + \rho_G) + \frac{g d_{eq}}{2}}} \tag{12}$$

CFD modeling

In this study, the $k-\varepsilon$ model was adopted for the simulation because it exhibits better stability, simplicity, and fast convergence [15]. It includes the additional equation for the Reynolds stress and the transport equation for the turbulent kinetic energy and dissipation rate [16]. The model is suitable for flows with complex secondary flow characteristics [17]. The standard $k-\varepsilon$ equation is used considering the physics of the flow and precision. The following equations are solved for transport:

$$\frac{\partial}{\partial t}(\alpha_k \rho_k \mathrm{k}_k) + \nabla.(\alpha_k \rho_k \mathrm{u}_k . \mathrm{k}_k) = \nabla(\alpha_k(\mu_k + \frac{\mu_{T,k}}{\sigma_k})\nabla \mathrm{k}_k) + \alpha_k(\mathrm{G}_{k,k} - \rho_k \varepsilon_k) + \mathrm{S}_{k,k} \tag{13}$$

$$\frac{\partial}{\partial t}(\alpha_k \rho_k \varepsilon_k) + \nabla.(\alpha_k \rho_k \mathrm{u}_k . \varepsilon_k) = \nabla(\alpha_k(\mu_k + \frac{\mu_{T,k}}{\sigma_\varepsilon})\nabla \varepsilon_k) + \alpha_k \frac{\varepsilon_k}{k_k}(\mathrm{C}_{1\varepsilon} G_{k,k} - C_{2\varepsilon}\rho_k \varepsilon_k) + C_{3\varepsilon}\frac{\varepsilon_k}{k_k}\mathrm{S}_{k,k} \tag{14}$$

where $\mu_{T,k}$ is turbulent viscosity, which is defined as follows:

$$\mu_{T,k} = \rho_p C_\mu \frac{k_k^2}{\varepsilon_k} \tag{15}$$

Table 2 Values used in the k–ε model

Constant	C_μ	$C_{1\varepsilon}$	$C_{2\varepsilon}$	$C_{3\varepsilon}$	σ_k	σ_ε
Value	0.09	1.44	1.92	1.2	1.0	1.3

The two-fluid Euler–Euler model [18, 19] is used to solve the equations for each phase. Adiabatic flow is considered; thus, the continuity and momentum equations for both phases are employed.

$$\frac{\partial}{\partial t}\left(\alpha_k \rho_k\right) + \frac{\partial}{\partial x_i}\left(\alpha_k \rho_k U_{i,k}\right) = 0 \tag{16}$$

$$\frac{\partial}{\partial t}\left(\alpha_k \rho_k U_{i,k}\right) + \frac{\partial}{\partial x_j}(\alpha_k \rho_k U_{i,k} U_{j,k}) = -\alpha_k \frac{\partial}{\partial x_i} p_k + \frac{\partial}{\partial x_j}\left[\alpha_k \left(\tau_{ij,k} + \tau_{ij,k}^{Re}\right)\right] + \alpha_k \rho_k g_i + M_k \tag{17}$$

α_k represents the volume fraction of phase k. g is the gravitational acceleration. τ and τ^{Re} are the laminar and turbulent stress tensors, respectively. M_k represents the momentum exchanges between the phases.

The interfacial momentum forces in Eq. (17) account for the interactions between the continuous and dispersed phases.

The drag, lift, and turbulent dispersion forces are the important interfacial forces for gas–liquid flows under the Euler–Euler approach.

M_D is considered as the drag per unit volume, which is represented by the following equation:

$$\vec{M}_D = \frac{3}{4}\alpha_g \rho_L \frac{C_D}{d_b}\left|\vec{u}_L - \vec{u}_G\right|\left(\vec{u}_L - \vec{u}_G\right) \tag{18}$$

where α_g represents the gas volume fraction and d_b is the diameter of a bubble. Ishii and Zuber [20] proposed several correlations for the drag coefficient, C_D, of individual bubbles for distinct Reynolds number regions. These correlations are as follows:

$$C_D(sphere) = \frac{24}{Re_b}\left(1 + 0.15Re_b^{0.678}\right) \tag{19}$$

$$C_D(ellipse) = \frac{2}{3}Eo^{1/2} \tag{20}$$

$$C_D(cap) = \frac{8}{3} \tag{21}$$

where the Reynolds and Eötvös numbers of the bubbles are defined as

$$Re_b = \frac{\rho_L\left|u_L - u_G\right|d_{eq}}{\mu_L} \tag{22}$$

$$Eo = \frac{g\left(\rho_L - \rho_G\right) d_{eq}^2}{\sigma} \tag{23}$$

Finally, the flow regime is selected as follows:

$$C_D = \max\left\{ C_D\left(sphere\right), \min\left[C_D\left(ellipse\right), C_D\left(cap\right)\right]\right\} \tag{24}$$

Let $n(v,t)$ represent the number density of bubbles with size v at time t. Then, the population balance model is used to describe the coalescence and breakup of bubbles, which is given by [21]

$$\frac{\partial n(v,t)}{\partial t} + \nabla\cdot(\mathrm{u}_g\, \mathrm{n}(v,\mathrm{t})) = B_C + B_B - D_C - D_B \tag{25}$$

where B_C represents the birth rate due to the coalescence of small bubbles, B_B is the birth rate due to the breakup of large bubbles, D_C is the death rate due to coalescence with other bubbles, and D_B represents the death rate due to breakup into small bubbles.

These rates can be expressed as [22]

$$B_B = \int_v^\infty \mathrm{g}(\varepsilon; v) n(v,t) d\varepsilon \tag{26}$$

$$B_C = \frac{1}{2}\int_0^v \mathrm{Q}(v-\varepsilon;\varepsilon) n(v-\varepsilon,t) n(v,t) d\varepsilon \tag{27}$$

$$D_B = n(v,t)\int_0^v g(v;\varepsilon)d\varepsilon \tag{28}$$

$$D_C = n(v,t)\int_0^\infty Q(v;\varepsilon)n(\varepsilon,t)d\varepsilon \tag{29}$$

where $g(v;\varepsilon)$ and $Q(v;\varepsilon)$ represent the specific breakup and coalescence rates, respectively. Then, the population balance equation is discretized into different size groups. Let N_i represent the number density of size group i.

$$N_i(t) = \int_{v_i-\frac{1}{2}}^{v_i+\frac{1}{2}} n(v,t)dt \tag{30}$$

The size distribution is discretized into a predefined set of size groups. The discretization is controlled by user-defined diameters, and the diameters are converted to masses using the reference density. Equal-diameter discretization is used for creating size groups. The diameter of group *i* is calculated as

$$d_i = d_{\min} + \Delta d\left(i - \frac{1}{2}\right) \tag{31}$$

$$\Delta d = \frac{d_{\max} - d_{\min}}{N} \tag{32}$$

The relationship between the diameter and mass of a particular group is given by

$$m = \rho_G \frac{\pi d^3}{6} \tag{33}$$

The bubble breakup rate in terms of mass can be obtained as

$$r\left(M_i,M_j\right)=\mathrm{C}(1-\alpha_g)(\frac{\varepsilon}{d_j{}^2})^{\frac{1}{3}}\int_{\xi_{\min}}^{1}\frac{(1+\xi)^2}{\xi^{\frac{11}{3}}}\times\exp\left(-\frac{12c_f\sigma}{\beta\rho^l(\varepsilon^l)^{\frac{2}{3}}d^{\frac{5}{3}}\xi^{\frac{11}{3}}}\right)d\xi \tag{34}$$

where $\xi=\lambda/d_j$ is the size ratio between an eddy and a particle in the inertial subrange. Consequently, $\xi_{mi}=\lambda_{\min}/d_j$. C = 0.923 and β = 2.0 are determined from the fundamental consideration of the breakup of drops or bubbles in turbulent dispersion systems. The latter is adopted in this study.

Prince and Blanch [23] proposed the following correlation to express the coalescence rate in terms of mass:

$$a\left(M_i,M_j\right)=\frac{\pi}{4}\left[d_i+d_j\right]^2\left(u_{ti}{}^2+u_{tj}{}^2\right)^{0.5}\exp\left(-\frac{t_{ij}}{\tau_{ij}}\right) \tag{35}$$

where τ_{ij} is the contact time for two bubbles, which is given by $\left(d_{ij}/2\right)^{\frac{2}{3}}/\left(\varepsilon^l\right)^{\frac{1}{3}}$. t_{ij} is the time required for two bubbles with diameters d_i and d_j to coalesce. t_{ij} is estimated to be $\left[\left(\frac{d_{ij}}{2}\right)^3\rho^l/16\sigma\right]^{0.5}\ln\left(\frac{h_0}{h_f}\right)$ [24]. Equivalent diameter d_{ij} is calculated

according to the correlation proposed by Chesters and Hoffman: $d_{ij} = \left(\frac{2}{d_i} + \frac{2}{d_j} \right)^{-1}$. For air–water systems, Prince and Blanch experimentally determined the initial film thickness, h_0, and the critical film thickness, h_f, at which rupture occurred as 10^{-4} and 10^{-8} m, respectively. The turbulent velocity, u_t, in the inertial subrange of isotropic turbulence is given by

$$u_t = \sqrt{2}(\varepsilon^f)^{1/3} d_i^{1/3} \tag{36}$$

The equal-diameter model was used for the size group distribution. The bubble diameter ranged from 0.5 mm to 25 mm. The ‘‘velocity inlet’’ boundary conditions were used at the gas sparger and the ‘‘opening outlet’’ conditions at the outlet. The inlet velocity was maintained such that the superficial gas velocity ranged from 0.0056 m/s to 0.05 m/s. The entire computational domain was divided into more than two million unstructured hexahedral cells. Table 3 shows the number of cells for various reactor sizes. Simulation demonstrated that the solution was independent of the mesh size. The transient gas–liquid flow simulation method was used, and the time step was set as 5×10^{-4}–3×10^{-2} s. Simulation showed that the results were not sensitive to the time step within this range. Therefore, the time step was set as 2×10^{-2} s. Initially, the reactor was filled with the liquid. More than 10^4 steps were required to achieve convergence for each case. The liquid density and gas density were 1090 kg/

m³ and 20 kg/m³, respectively. The liquid viscosity was 0.18 Pa.s, which corresponded to an actual temperature of 160 °C.

Table 3 Number of cells for different heights of the airlift reactor

Reactor height	5 m	10 m	15 m	20 m	25 m
Number of cells	2060468	2152327	2276425	2441658	2658137

Hydrodynamic parameters

To investigate the local hydrodynamic parameters, the riser was divided into six equal parts, each with height h, starting from the top of H_2, as shown in Fig. 1. Therefore, seven cross sections along the riser were obtained. The bottom cross section was the first cross section.

The liquid circulation velocity in the airlift reactor mainly originates from the gas holdup difference between the riser and downcomer.

The contours of the gas holdup, liquid axial velocity, and bubble diameter were used to illustrate the hydrodynamics. The influence of the total height of the reactor, H, and the superficial gas velocity, $U_{Gr1} = Q_{G,in} / A_r$, due to gas injection on the hydrodynamics was discussed.

Results and discussion

Gas holdup

We define the area-averaged value of the gas holdup at a cross section of the riser as

ε_a. The total gas holdup is defined as the volume-averaged gas holdup in the riser zone.

Fig. 2 shows the contours of the gas holdup in the riser at different superficial velocities and a total reactor height of 15 m. The gas holdup increases with the superficial gas velocity. The gas holdup at the center of the riser is larger than that on the sidewalls of the riser. The gas holdup in the downcomer region is smaller than that in the riser.

Fig. 3 shows the gas holdup distribution at different total heights of the reactor and a superficial gas velocity of 0.0389 m/s. The gas holdup exhibits similar distributions for different total heights.

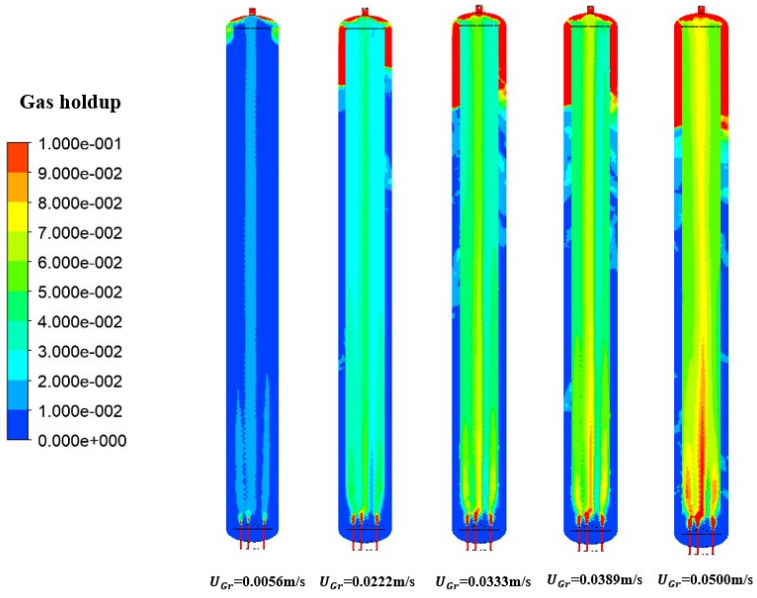

Fig. 2 Gas holdup distribution at different superficial gas velocities and total reactor height of 15 m

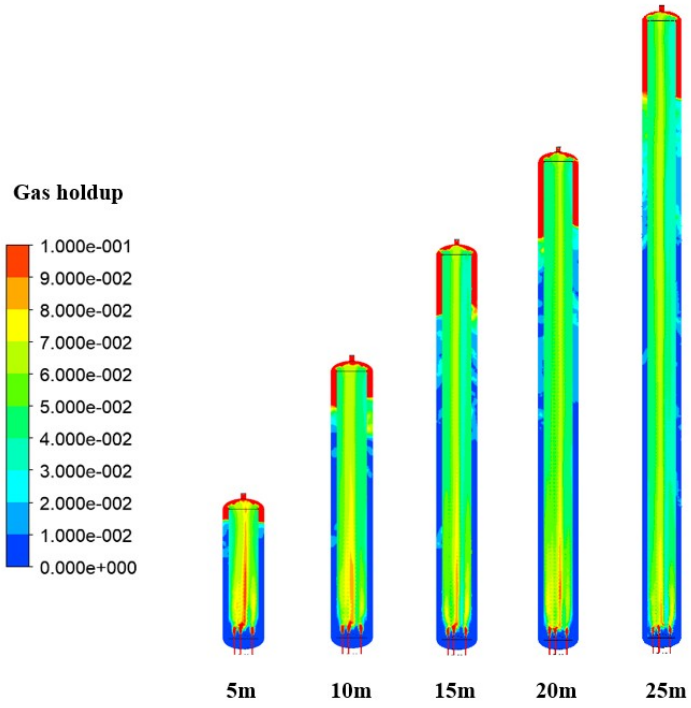

Fig. 3 Gas holdup distribution at different total reactor heights and superficial gas velocity of 0.0389 m/s

The gas is enriched at the top region of the downcomer, and the bottom region of the downcomer contains a negligible amount of the gas. This is in agreement with flow regime II according to Heijnen et al. [25]. The bubble-enriched zone in the downcomer in the reactor with a height of 5 m is smaller than that in the reactor with a height of 25 m. The displacement of the bubbles in the downcomer tends to increase with the total reactor height.

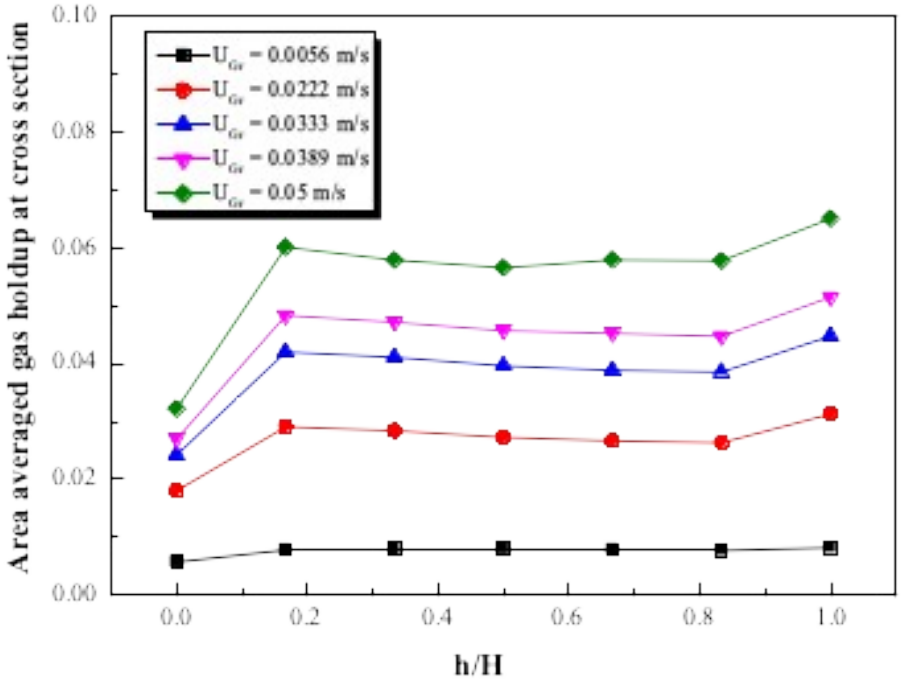

Fig. 4 Area-averaged gas holdup at different cross sections for various superficial gas velocities and total reactor height of 15 m

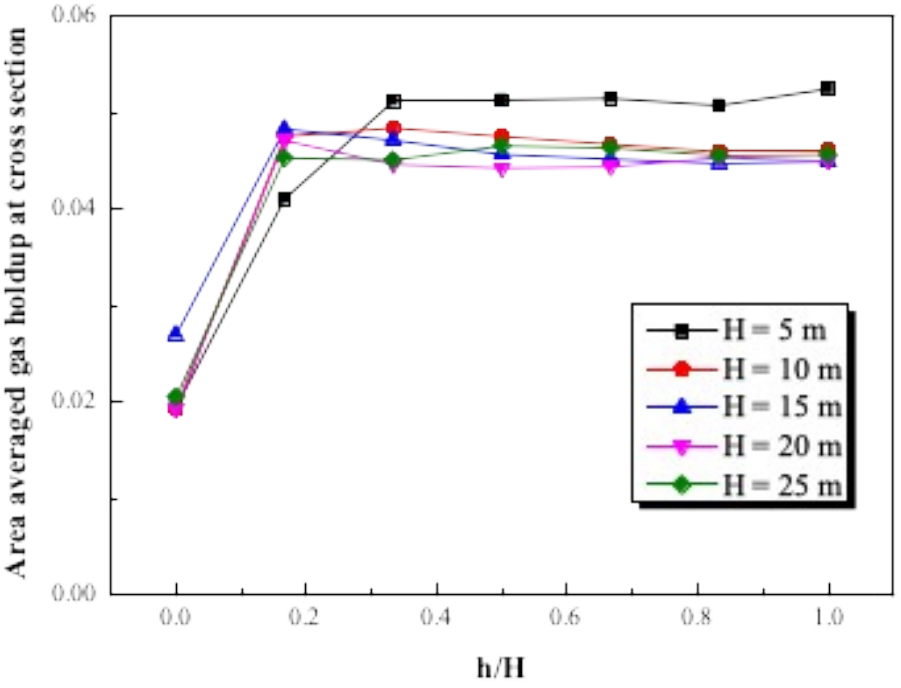

Fig. 5 Area-averaged gas holdup at different cross sections for various total reactor heights

and superficial gas velocity of 0.0389 m/s

Fig. 4 shows the area-averaged gas holdup at the cross sections (local heights) of the riser at different superficial gas velocities and a total reactor height of 15 m. As the local height increases, the area-averaged gas holdup first increases, then decreases, and finally increases again. The area-averaged gas holdup is almost constant in the riser region between the second and sixth cross sections.

Fig. 5 shows the area-averaged gas holdup at the cross sections (local heights) of the riser at different total reactor heights and a superficial gas velocity of 0.0389 m/s. The area-averaged gas holdup increases with the superficial gas velocity, and the trends of the increase are similar for different total reactor heights. According to Fig. 4 and Fig. 5, the gas holdup is the lowest at the first cross section, which is close to the gas inlet. This indicates the undeveloped multiphase flow at this location.

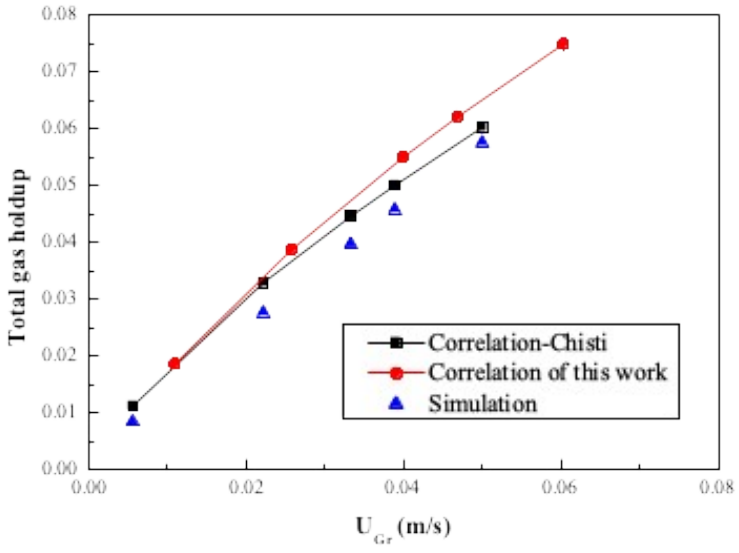

Fig. 6 Total gas holdup in riser calculated from correlations and CFD simulation at different superficial gas velocities

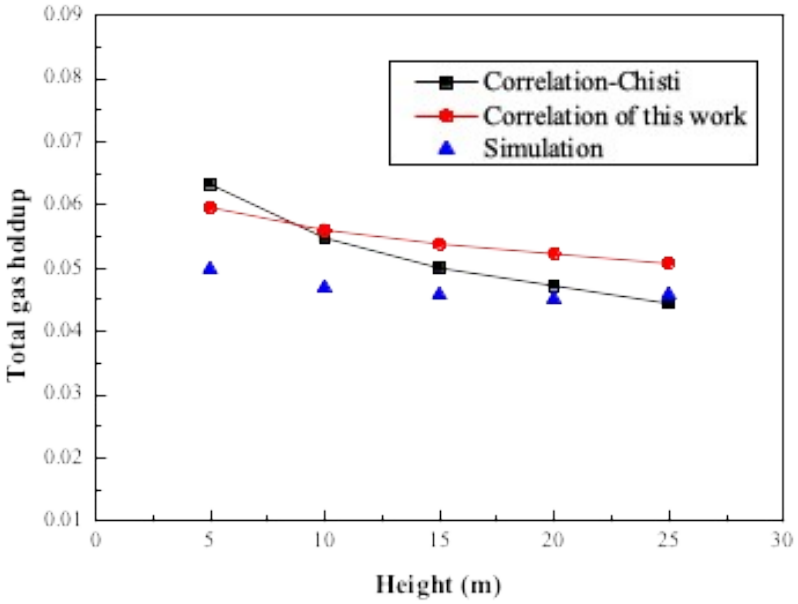

Fig. 7 Total gas holdup in riser calculated from correlations and CFD simulation at different total reactor heights

The comparison of the total gas holdup obtained using the Chisti correlation [26], the correlation proposed in this study, and the CFD simulation results is shown in Fig. 6 and Fig. 7. Fig. 6 shows the results for different superficial gas velocities and a total reactor height of 15 m. The total gas holdup obtained using the simulation and proposed correlation is lower and higher than that calculated by the Chisti correlation, respectively. Fig. 7 shows the results for different total reactor heights and a superficial gas velocity of 0.0389 m/s. The total gas holdup obtained using the simulation is slightly lower than that obtained using the two correlations. The simulation results are consistent with the results of this work, and the overall fitting results are satisfactory.

Although the proposed correlation considers the bubble diameter to enhance the reliability of the calculation results, it assumes that bubbles enter from the downcomer

into the riser at the bottom of the reactor. This is the reason that the value is larger. The proposed correlation may be more suitable for other gas–liquid conditions because the gas holdup is also affected by physical parameters and operating parameters, such as liquid viscosity [27], liquid surface tension, temperature, and pressure.

Liquid circulation velocity

The liquid circulation velocity is defined as the value of the superficial liquid velocity in the riser. The liquid circulation velocity is an important hydrodynamic parameter of the airlift reactor, and it is caused by the gas holdup difference between the riser and downcomer. The liquid circulation velocity is related to the axial liquid velocity and gas holdup in the riser, as follows: $U_{Lr} = V_{Lr}(1-\varepsilon_r)$, where V_{Lr} is the axial liquid velocity and ε_r is the gas holdup.

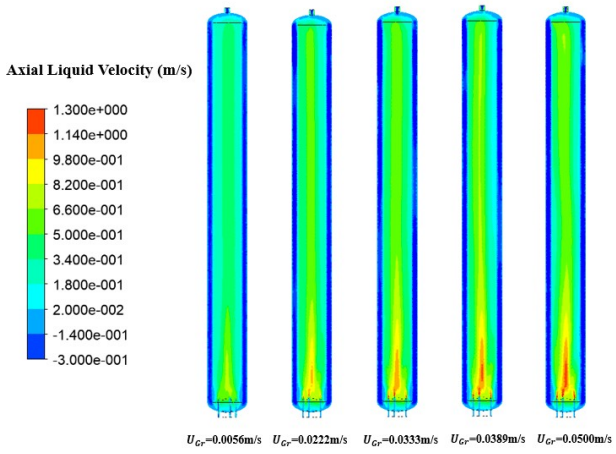

Fig. 8 Axial liquid velocity distribution at different superficial gas velocities and total reactor height of 15 m

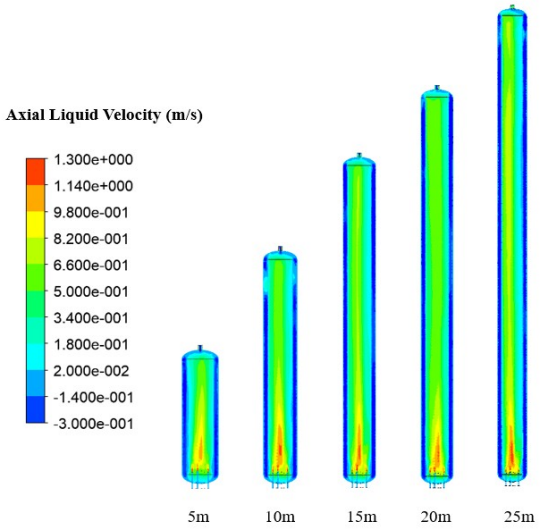

Fig. 9 Axial liquid velocity distribution at different total reactor heights and superficial gas velocity of 0.0389 m/s

Fig. 8 shows the contours of the axial liquid velocity at different superficial gas velocities and a total reactor height of 15 m. The axial liquid velocity increases with the superficial gas velocity. The growth rate of the axial liquid velocity decreases when the superficial gas velocity is larger than 0.0333 m/s. Fig. 9 shows the contours of the axial liquid velocity at different total reactor heights and a superficial gas velocity of 0.0389 m/s. The axial liquid velocity increases with the total reactor height. This is because as the total reactor height increases, the hydrostatic pressure increases, and consequently, the pressure difference between the riser and downcomer increases. This results in an increase in the liquid circulation velocity.

When the superficial gas velocity increases, the liquid circulation velocity gradually

increases when the gas holdup is high; this has been reported by previous studies [28-31]. This is because the displacement of the bubbles in the downcomer tends to increase with the superficial gas velocity. As seen from Fig. 2, the gas holdup difference between the riser and downcomer decreases as the superficial gas velocity increases. Finally, the growth rate of the liquid circulation velocity decreases as the superficial gas velocity increases.

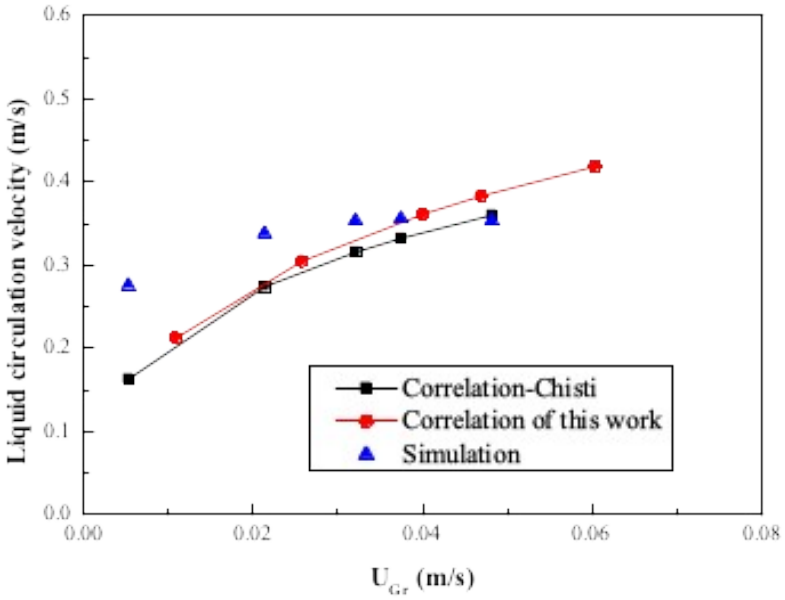

Fig. 10 Liquid circulation velocity calculated from correlations and CFD simulation at different superficial gas velocities

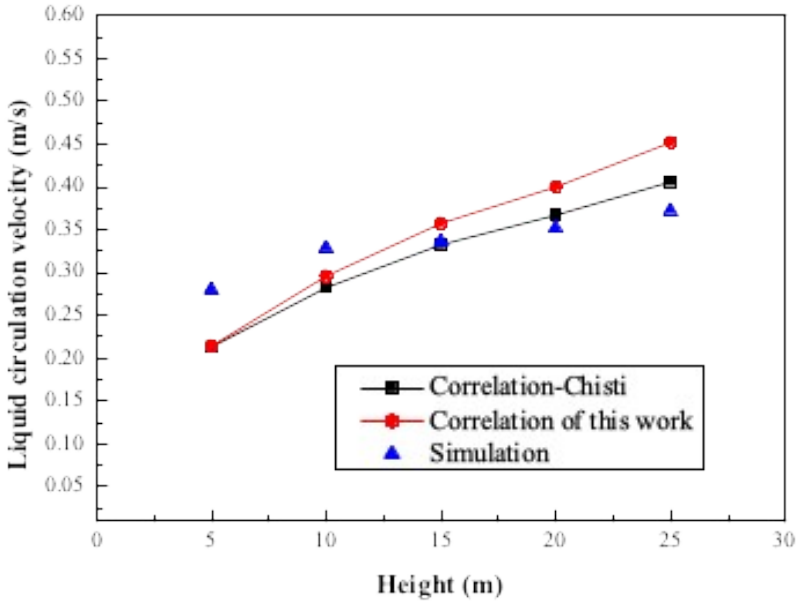

Fig. 11 Liquid circulation velocity calculated from correlations and CFD simulation at different total reactor heights

The comparison of the liquid circulation velocity obtained using the Chisti correlation, proposed correlation, and simulation is shown in Fig. 10 and Fig. 11. Fig. 10 shows the results for different superficial gas velocities and a total reactor height of 15 m. When the superficial gas velocity is lower than 0.0389 m/s, the simulation results are larger than the results obtained using the two correlations.

Fig. 11 shows the results for different total reactor heights and a superficial gas velocity of 0.0389 m/s. The results obtained using the Chisti correlation fit the simulation results well, and the results obtained using the proposed correlation are slightly larger than the simulation results. The results obtained using the two correlations exhibit the same variation trends. When the total reactor height is less than 10 m and more than 15 m, the simulation results are larger and smaller than the results obtained using the two correlations, respectively.

Bubble diameter

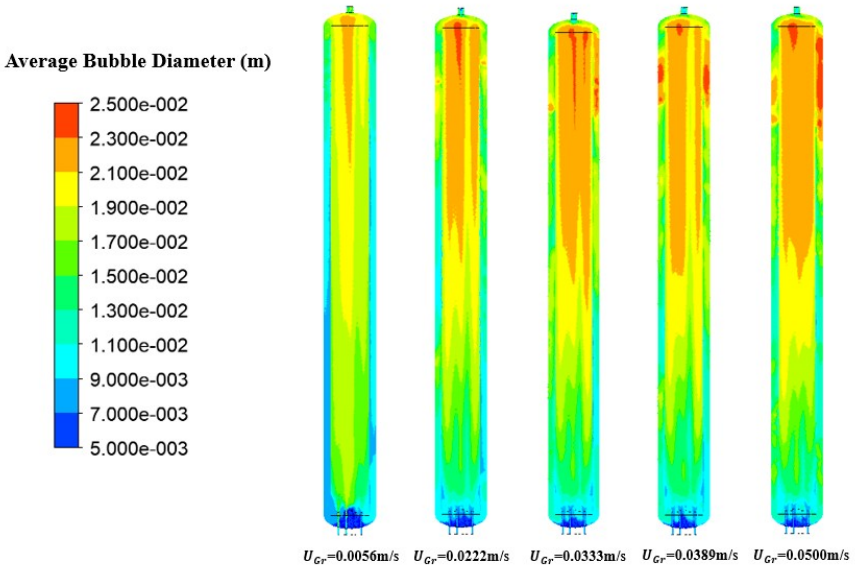

Fig. 12 Average bubble diameter distribution at different superficial gas velocities and total reactor height of 15 m

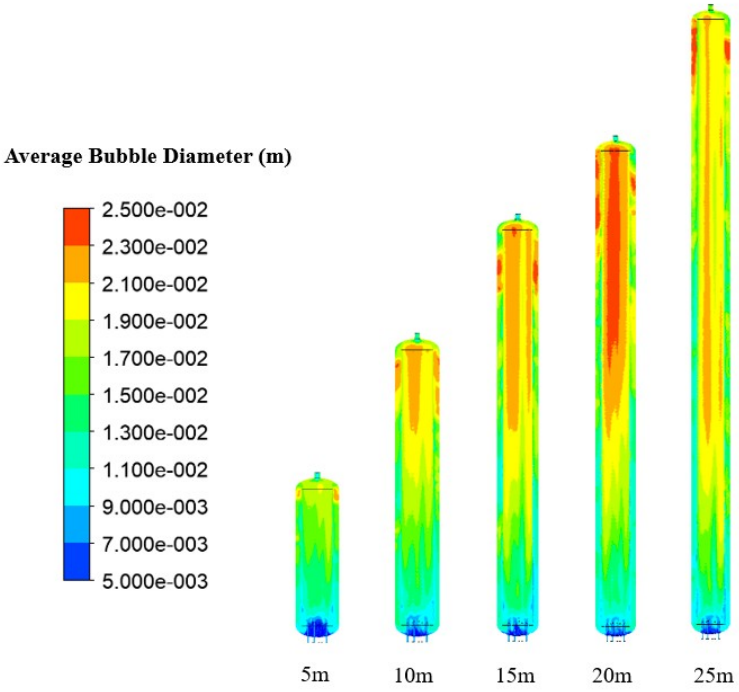

Fig. 13 Average bubble diameter distribution at different total reactor heights and superficial gas velocity of 0.0389 m/s

The equilibrium value of the average bubble diameter is determined by the local hydrodynamic conditions. The well-known correlation for the bubble diameter is as follows [32, 33]

$$d_B = 4.15\varepsilon_r^{0.5}\frac{\sigma^{0.6}}{\varepsilon^{0.4}\rho^{0.2}} + 0.0009 \quad (37)$$

The bubble diameter distribution is an important parameter of hydrodynamics, which depends on the coalescence and breakup of bubbles [34]. Fig. 12 shows the average bubble diameter distribution in the riser for different superficial gas velocities and a total reactor height of 15 m. The bubble diameter gradually increases from the bottom to the top of the reactor, and the large bubbles in the downcomer are mainly concentrated at the top. The bubble diameter at the middle and bottom of the downcomer is smaller than that in the riser. Fig. 13 shows the average bubble diameter distribution in the riser for different total reactor heights and a superficial gas velocity of 0.0389 m/s. As the total reactor height increases, the average bubble diameter gradually increases up to a height of 20 m and decreases when the height is 25 m.

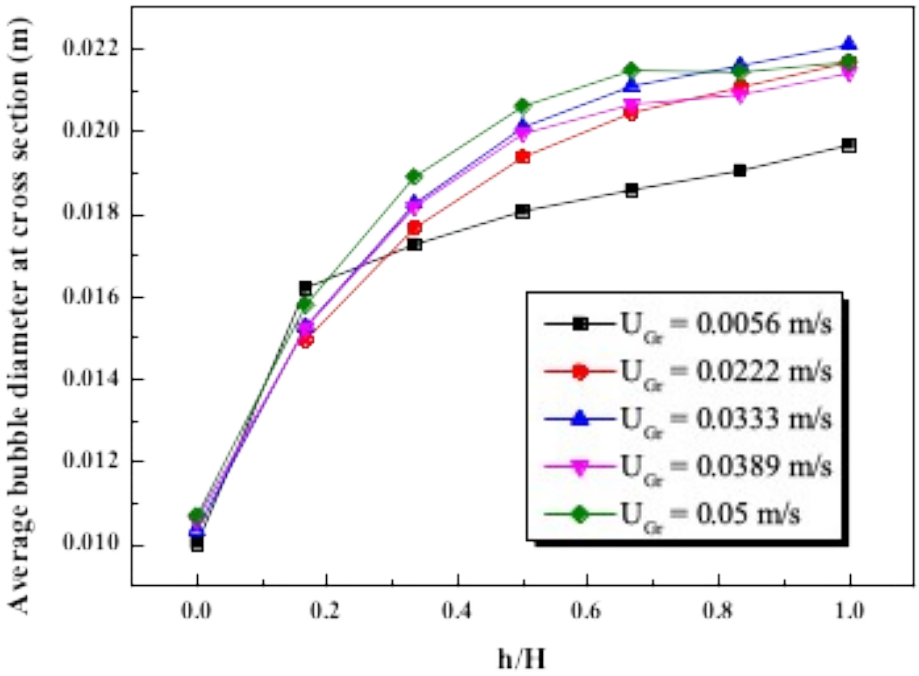

Fig. 14 Average bubble diameter at different cross sections at various superficial gas velocities and total reactor height of 15 m

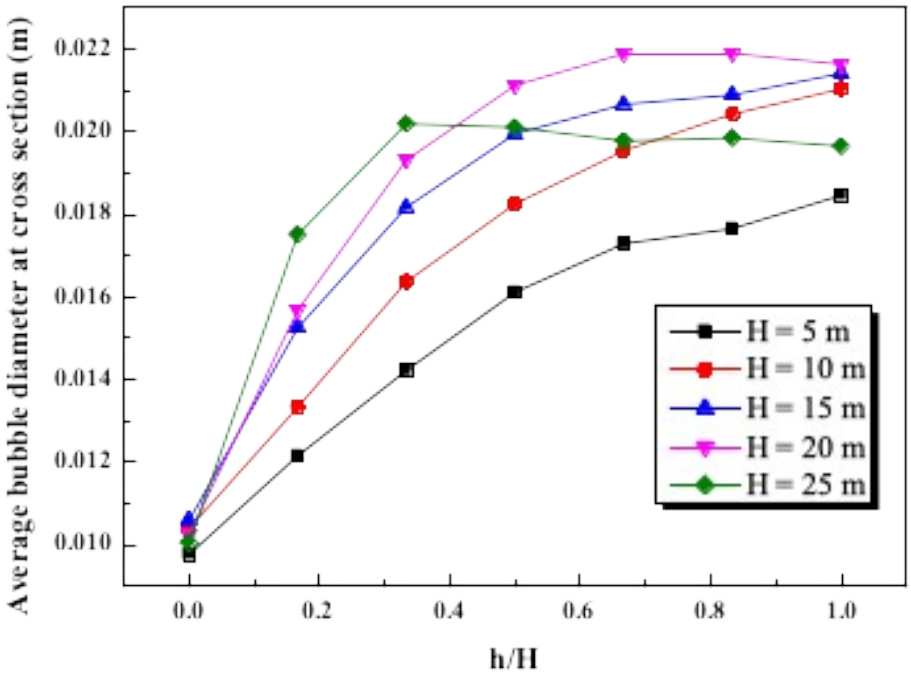

Fig. 15 Average bubble diameter at different cross sections at various total reactor heights

and superficial gas velocity of 0.0389 m/s

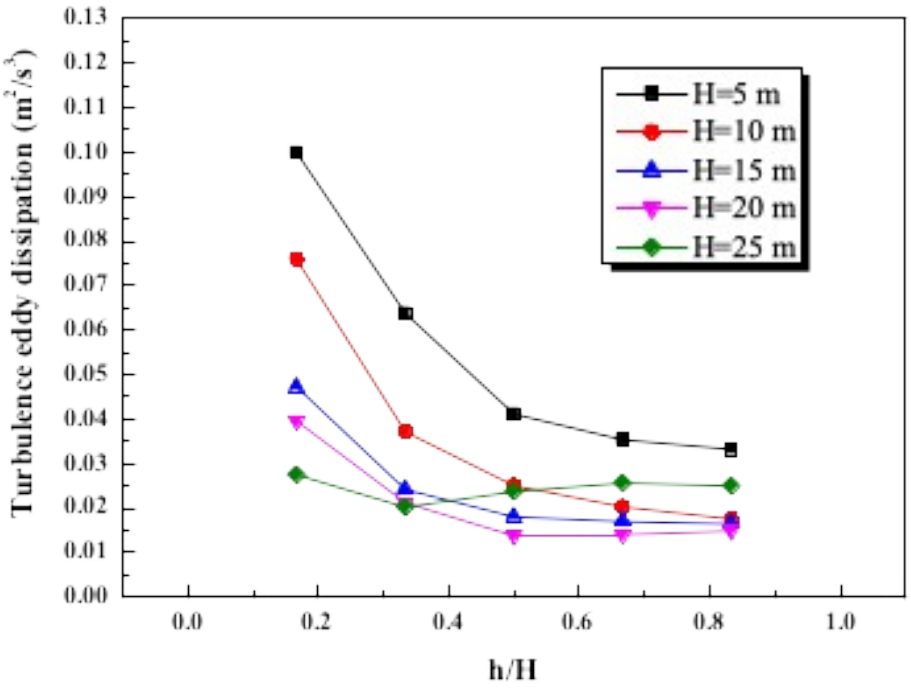

Fig. 16 Turbulent eddy dissipation at different cross sections at various total reactor heights and superficial gas velocity of 0.0389 m/s

The average bubble diameter at different cross sections was analyzed to investigate the change in the average bubble diameter along the axial direction of the reactor. Fig. 14 shows the average bubble diameter at different cross sections for various

superficial gas velocities and a total reactor height of 15 m. The average bubble diameter gradually increases from 10 mm to 22 mm from the first to seventh cross section. The growth rate of the bubble diameter gradually decreases with the local height, and the growth rate from the first to third section is high. When the superficial gas velocity is 0.0056 m/s, the average bubble diameter from the second section onwards is lower than that at other superficial gas velocities. The average bubble diameter does not increase significantly when the superficial gas velocity is more than 0.0222 m/s.

Fig. 15 shows the average bubble diameter at different cross sections for various total reactor heights and a superficial gas velocity of 0.0389 m/s. The average bubble diameter increases with the local height up to a total reactor height of 20 m. In addition, the growth rate of the bubble diameter from the first to third section increases with the total reactor height. At total reactor heights of 20 m and 25 m, the bubble diameter decreases from the fifth and third section onwards, respectively. This is investigated on the basis of the turbulent dissipation in each section. Fig. 16 shows the turbulent eddy dissipation at different cross sections for various total reactor heights and a superficial gas velocity of 0.0389 m/s. When the gas holdup is constant, the bubble diameter has a negative correlation with turbulent dissipation. Here, the unstable top and bottom sections are not considered. When the total reactor height is 25 m, the turbulent dissipation significantly increases from the third section onwards. This is an important reason for the decrease in the average bubble diameter.

Conclusion

The hydrodynamic characteristics of an industrial-scale internal loop airlift reactor are studied based on a molten sulfur system with high viscosity using the three-dimensional transient Euler multiphase-flow standard k–ε model coupled with the population balance model. An optimized correlation for the gas holdup and liquid circulation velocity is proposed; the correlation considers the influence of the bubble diameter. The effects of the superficial gas velocity and reactor height on the gas holdup, liquid circulation velocity, and average bubble diameter are examined. The CFD simulation results are compared with the results obtained using the Chisti correlation and proposed correlation.

At a total reactor height of 15 m, the gas holdups in the riser and downcomer increase with the superficial gas velocity. The liquid circulation velocity increases with the superficial gas velocity. The growth rate of the liquid circulation velocity decreases along with the superficial gas velocity when the superficial gas velocity is larger than critical value. The average bubble diameter slightly increases with the superficial gas velocity. When the superficial gas velocity is more than 0.0333 m/s, the bubble diameter decreases in the upper part of the reactor. The reason for this is as follows: As the superficial gas velocity increases, the turbulence degree of the reactor increases, the maximum stable bubble diameter decreases, and thus, the average bubble diameter decreases [35, 36]. A few studies have shown that the average bubble diameter slightly increases with the superficial gas velocity [37]. There is a maximum stable bubble diameter at a critical value of the superficial gas velocity. When the

superficial gas velocity is less than the critical value, the average bubble diameter slightly increases with the superficial gas velocity. However, when the superficial gas velocity is more than the critical value, severe bubble breakup occurs and the average bubble diameter decreases.

When the superficial gas velocity is 0.0389 m/s, as the total reactor height increases from 5 m to 25 m, there is no evident change in the gas holdup, but the number of bubbles in the downcomer increases. The liquid circulation velocity increases with the total reactor height. In addition, it is affected the gas holdup difference between the riser and downcomer and the hydrostatic pressure of the liquid column. The average bubble diameter increases with the total reactor height, and it decreases when the total reactor height reaches a critical value. When the total reactor height and superficial gas velocity are large, turbulent dissipation is an important factor that affects the bubble diameter.

The optimized correlation appears to be reasonable compared with the Chisti correlation and simulation. In addition, the more information, such as bubble diameter, was improved well.

In terms of the prediction of the gas holdup and liquid circulation velocity, the CFD simulation results are slightly different from the results obtained using the Chisti correlation and proposed correlation. However, the overall comparison results are acceptable. The application of the Chisti correlation is limited to the cases in which the maximum height of the reactor is 8.5 m (external loop airlift reactor) and the maximum diameter of the riser is 0.407 m. The CFD simulation provide detailed

information about the hydrodynamics, which is beneficial for evaluating the two correlations. The results obtained using both correlations agree with the CFD simulation results. This work has a positive influence on the fundamentals of designing aeration airlift reactors.

Notations

A_b	free area for liquid flow between the riser and downcomer, m^2
A_d	cross-sectional area of the downcomer, m^2
A_r	cross-sectional area of the riser, m^2
B_B	birth rate due to break-up
B_C	birth rate due to coalescence
C	break-up model constant
C_d	distribution parameter
C_D	drag coefficient
$C_{1\varepsilon}$	model parameter in turbulent energy dissipation equation
$C_{2\varepsilon}$	model parameter in turbulent energy dissipation equation
$C_{3\varepsilon}$	model parameter in turbulent energy dissipation equation
C_μ	constant parameter in *k*–ε model
c_f	coefficient of surface area
D_B	death rate due to break-up
D_C	death rate due to coalescence
D_r	riser diameter, m
d_B	Sauter mean diameter, m
d_b	diameter of the bubble, m
d_{eq}	bubble equivalent diameter, m
f	friction factor
G_k	production of turbulent kinetic energy, $kg \cdot m^{-1}s^{-3}$

g	gravitational acceleration, $m \cdot s^{-2}$
h_D	gas-liquid dispersion height, m
h_f	critical film thickness, m
h_o	initial film thickness, m
K_B	frictional loss coefficient (bottom)
k	turbulence kinetic energy, $m^2 \cdot s^{-2}$
$Q_{G,\in ¿ ¿}$	inlet gas flow rate, $m^3 \cdot s^{-1}$
$\Re_b$	bubble Reynolds number
r $(M_i, M_j$	break-up rate in terms of mass
)	
S_k	source terms
t_{ij}	time for two bubbles to coalesce, s
U_b	bubble terminal velocity, $m \cdot s^{-1}$
U_{Gr}	superficial gas velocity (riser), $m \cdot s^{-1}$
U_{Lr}	superficial liquid velocity (riser), $m \cdot s^{-1}$
U_{Gd}	superficial gas velocity (downcomer), $m \cdot s^{-1}$
U_{Ld}	superficial liquid velocity (downcomer), $m \cdot s^{-1}$
u	velocity, $m \cdot s^{-1}$
$\vec{u_L}$	local liquid phase velocity, $m \cdot s^{-1}$
$\vec{u_G}$	local gas phase velocity, $m \cdot s^{-1}$
V_{Lr}	liquid axial velocity, $m \cdot s^{-1}$
α_g	gas volume fraction
β	break-up kernel constant

ε	turbulence kinetic energy dissipation
ε_r	gas holdup (riser)
ε_d	gas holdup (downcomer)
μ	Viscosity, Pa·s
μ_L	liquid phase dynamic viscosity, Pa·s
μ_T	turbulence viscosity
ξ	size ratio between an eddy and a particle
ρ	density, kg·m^{-3}
ρ_G	gas phase density, kg·m^{-3}
ρ_L	liquid phase density, kg·m^{-3}
σ	surface tension, N/m
σ_k	constant in k-ε model
σ_ε	constant in k-ε model
τ	laminar stress tensors
$\tau^{\Re}$	turbulent stress tensors
τ_{ij}	contact time for two bubbles, s

References

[1] S. Ibrahim, R.K. Rahman, A. Raj, Roles of hydrogen sulfide concentration and fuel gas injection on aromatics emission from Claus furnace, Chemical Engineering Science 172 (2017) 513-527.
[2] F. Tari, M. Shekarriz, S. Zarrinpashne, A. Ruzbehani, Design and implementation of an effective system for catalytic degassing of claus-derived molten sulfur over monometallic and bimetallic nanosilica-based catalysts and optimization via RSM-CCD, Journal of Natural Gas Science and Engineering 59 (2018) 124-135.
[3] M.Y. Chisti, B. Halard, M. Moo-Young, Liquid circlulation in airlift reactor, Chemical Engineering Science 43 (1988) 451-457.
[4] A.E. Saez, M.A. Marquez, G.W. Roberts, R.G. Carbonell, Hydrodynamic Model for Gas-Lift Reactors, AIChE Journal 44 (1998) 1413-1423.
[5] H.Dhaouadi, S.Poncin, J.M.Hornut, G.Wild, P.Oinas, J.Korpijarvi, Mass transfer in an external-loop airlift reactor: experiments and modeling, Chemical Engineering Science 52 (1997) 3909-3917.
[6] T.J. Lin, K. Tsuchiya, L.S. Fan, Bubble Flow Characteristics in Bubble Columns at Elevated Pressure and Temperature, AIChE Journal 44 (1998) 545-560.
[7] G. Besagni, F. Inzoli, The effect of liquid phase properties on bubble column fluid dynamics: Gas holdup, flow regime transition, bubble size distributions and shapes, interfacial areas and foaming phenomena, Chemical Engineering Science 170 (2017) 270-296.
[8] P.M. Wilkinson, H. Haringa, L.L.V. Dierendonck, Mass transfer and bubble size in a bubble column under pressure, Chemical Engineering Science 49 (1994) 1417-1427.
[9] N. Zuber, J.A. Findlay, Average volumetric concentration in two-phase flow systems, Journal of Heat Transfer 87 (1965) 453-468.
[10] S.-J. Hwang, Yi-LungCheng, Gas holdup and liquid velocity in three-phase internal-loop airlift reactors, Chemical Engineering Science 52 (1997) 3949-3960.
[11] Y. Gao, D. Hong, H. Lu, Y. Cheng, L. Wang, X. Li, Gas holdup and liquid velocity distributions in the up flow jet-loop reactor, Chemical Engineering Research and Design 136 (2018) 94-104.
[12] L. Chriastel, Y. Kawase, H. Znad, Hydrodynamic Modelling of Internal Loop Airlift Reactor Applying Drift-Flux Model in Bubbly Flow Regime, The Canadian Journal of Chemical Engineering 85 (2007) 226-232.
[13] M. Jamialahmadi, C. Branch, H. Muller-Steinhagen, Terminal bubble rise velocity in liquids Chemical Engineering Research and Design 72 (1994) 119-122.
[14] Z. Tian, Y. Cheng, X. Li, L. Wang, Bubble shape and rising velocity in viscous liquids at high temperature and pressure, Experimental Thermal and Fluid Science 102 (2019) 528-538.
[15] D. Pfleger, S. Gomes, N. Gilbert, H.G. Wagner, Hydrodynamic simulations of laboratory scale bubble columns fundamental studies of the Eulerian–Eulerian modelling approach, Chem Eng Sci 54 (1999) 5091-5099.

[16] N. Moudoud, R. Rihani, F. Bentahar, J. Legrand, Global hydrodynamic of hybrid external loop airlift reactor: Experiments and CFD modelling, Chemical Engineering and Processing - Process Intensification 129 (2018) 118-130.
[17] C. Laborde-Boutet, F. Larachi, N. Dromard, O. Delsart, D. Schweich, CFD simulation of bubble column flows: Investigations on turbulence models in RANS approach, Chem Eng Sci 64 (2009) 4399-4413.
[18] T. Ziegenhein, R. Rzehak, T. Ma, D. Lucas, Towards a unified approach for modelling uniform and non-uniform bubbly flows, The Canadian Journal of Chemical Engineering 95 (2017) 170-179.
[19] T. Ziegenhein, R. Rzehak, D. Lucas, Transient simulation for large scale flow in bubble columns, Chemical Engineering Science 122 (2015) 1-13.
[20] M. Ishii, N. Zuber, Drag coefficient and relative velocity in bubbly, droplet or particulate flows, AIChE Journal 25 (1979) 843-855.
[21] S.C.P. Cheung, S. Vahaji, G.H. Yeoh, J.Y. Tu, Modeling subcooled flow boiling in vertical channels at low pressures – Part 1: Assessment of empirical correlations, International Journal of Heat and Mass Transfer 75 (2014) 736-753.
[22] P. Ranganathan, S. Sivaraman, Investigations on hydrodynamics and mass transfer in gas–liquid stirred reactor using computational fluid dynamics, Chemical Engineering Science 66 (2011) 3108-3124.
[23] M.J.P.H.W. Blanch, Bubble coalescence and break-up in air-sparged bubble columns, AIChE J (1990).
[24] G.H. Yeoh, S.C. Cheung, J.Y. Tu, On the prediction of the phase distribution of bubbly flow in a horizontal pipe, Chemical engineering research & design : transactions of the Institution of Chemical Engineers 90 (2012) 40-51.
[25] J.J. Heijnen, J. Hols, R.G.J.M. van der Lans, H.L.J.M. van Leeuwen, A. Mulder, R. Weltevrede, A simple hydrodynamic model for the liquid circulation velocity in a full-scale two- and three-phase internal airlift reactor operating in the gas recirculation regime, Chem Eng Sci 52 (1997) 2527-2540.
[26] Y. Chisti, M. Moo-Young, Improve the performance of airlift reactors, Chemical Engineering Progress 89 (1993) 38-45.
[27] K. Akita, F. Yoshida, Bubble size, interfacial area, and liquid-phase mass transfer coefficient in bubble columns, Industrial and Engineering Chemistry Process Design and Development 13 (1974) 84-91.
[28] G. Olivieri, A. Marzocchella, P. Salatino, Hydrodynamics and mass transfer in a lab-scale three-phase internal loop airlift, Chem Eng J 96 (2003) 45-54.
[29] Š. Godó, J. Klein, M. Polakovič, V. Báleš, Periodical changes of input air flowrate – a possible way of improvement of oxygen transfer and liquid circulation in airlift bioreactors, Chem Eng Sci 54 (1999) 4937-4943.
[30] K.H. Choi, Y. Chisti, M. Moo-Young, Comparative evaluation of hydrodynamic and gas—liquid mass transfer characteristics in bubble column and airlift slurry reactors, The Chemical Engineering Journal and the Biochemical Engineering Journal 62 (1996) 223-229.
[31] K. Akita, O. Nakanishi, K. Tsuchiya, Turn-around energy losses in an external-loop airlift reactor, Chem Eng Sci 49 (1994) 2521-2533.

[32] Z. Huang, D.D. McClure, G.W. Barton, D.F. Fletcher, J.M. Kavanagh, Assessment of the impact of bubble size modelling in CFD simulations of alternative bubble column configurations operating in the heterogeneous regime, Chemical Engineering Science 186 (2018) 88-101.
[33] B. Wang, G. Yang, H. Tian, X. Li, G. Yang, Y. Shi, Z. Zhou, F. Zhang, Z. Zhang, A new model of bubble Sauter mean diameter in fine bubble-dominated columns, Chemical Engineering Journal 393 (2020) 124673.
[34] T. Wang, J. Wang, Numerical simulations of gas–liquid mass transfer in bubble columns with a CFD–PBM coupled model, Chem Eng Sci 62 (2007) 7107-7118.
[35] P. Wongsuchoto, T. Charinpanitkul, P. Pavasant, Bubble size distribution and gas–liquid mass transfer in airlift contactors, Chem Eng J 92 (2003) 81-90.
[36] L.A. Glasgow, L.E. Erickson, C.H. Lee, Wall pressure fluctuations and bubble size distributions at several positions in an airlift fermentor, Chem Eng Commun 29 (1984) 311-336.
[37] R. Van Der Welle, Void fraction, bubble velocity and bubble size in two-phase flow, Int J Multiphas Flow 11 (1985) 317-345.